PHYSICAL REVIEW B **91**, 161110(R) (2015)

Anisotropic energy scale for degenerate Fermi and non-Fermi liquids near a quantum critical phase transition in $YbRh_2Si_2$

S. Kambe,[1] H. Sakai,[1] Y. Tokunaga,[1] G. Lapertot,[2] T. D. Matsuda,[1,*] G. Knebel,[2] J. Flouquet,[2] and R. E. Walstedt[3]

[1]*Advanced Science Research Center, Japan Atomic Energy Agency, Tokai-mura, Ibaraki 319-1195, Japan*

[2]*Service de Physique Statistique, Magnétisme et Supraconductivité, Institut Nanosciences et Cryogénie, CEA-Grenoble/Université J. Fourier Grenoble I, 17 rue des Martyrs, 38054 Grenoble, France*

[3]*Physics Department, The University of Michigan, Ann Arbor, Michigan 48109, USA*

(Received 19 January 2015; revised manuscript received 2 March 2015; published 24 April 2015)

Based on ^{29}Si nuclear spin-lattice relaxation time (T_1) data on a single crystal of $YbRh_2Si_2$, the coexisting Fermi liquid and non-Fermi liquid states around the quantum critical phase transition have been found to be sensitive to the direction of the applied magnetic field. Augmented scaling analysis shows that the anisotropic characteristic temperature and field are roughly ten times larger for $H\|c$ than for $H\|a$, consistent with a previously obtained anisotropic phase diagram.

DOI: 10.1103/PhysRevB.91.161110 PACS number(s): 71.27.+a, 76.60.−k

Quantum critical phase transitions (QCPTs) at $T = 0$ K in the heavy fermion state of a Kondo lattice offer various interesting aspects. In the heavy fermion system $YbRh_2Si_2$ [1–6], the QCPT is not the usual case of spin density wave (SDW) instability observed in Ce-based compounds [7], but a candidate for the novel locally critical QCPT case [8–10]. In $YbRh_2Si_2$, the weak antiferromagnetic transition below $T_N \sim 70$ mK is easily suppressed to $T = 0$ with a small applied magnetic field H [1]. Unfortunately, the antiferromagnetic ordering has not yet been confirmed, which may be due to the low T_N and a small ordered moment [11]. As a consequence of its tetragonal crystal structure (Fig. 1), the phase diagram and thus the electronic state of $YbRh_2Si_2$ have been found to be quite anisotropic [4,12,13]. Correspondingly, the critical magnetic fields for $T_N \sim 0$ K are $H_{cr} \sim 0.06$ and 0.66 T for $H \perp c$ and $H\|c$ axes, respectively, indicating that the effective energy scale for quantum criticality is ∼10 times larger for the $H\| c$ axis.

A sudden change in the Fermi surface volume has been suggested theoretically [9] in the vicinity of the locally critical QCPT. In fact, transport measurements suggest such a change in the Fermi surface [2,3,12,14]. On the other hand, recent angle-resolved photoemission spectroscopy (ARPES) measurements in $YbRh_2Si_2$ indicate no drastic change in the Fermi surface near the QCPT [15]. Thus, the nature of the QCPT in $YbRh_2Si_2$ is still under debate.

In our previous paper [16], coexisting static Fermi liquid (FL) and non-Fermi liquid (NFL) states near the QCPT in $YbRh_2Si_2$ were brought to light by means of ^{29}Si nuclear spin-lattice relaxation time (T_1) studies with an $H\|c$ axis. Here, in order to probe the anisotropy of the quantum critical state, possible two-state behavior has been probed again via T_1 studies with H along the a axis for 45 mK $\leqslant T \leqslant$ 300 K and 0.31 T $\leqslant H \leqslant$ 7.2 T. Similar, but somewhat more muted, behavior has been found with the field in the basal plane. The anisotropy of T_1 for the $H\|a$ and $H\|c$ cases at high temperatures has been discussed previously [13].

The same sample as used previously [13,16] has been employed in the present study. High sample purity has been confirmed by low residual resistivity $\rho_0 \sim 0.99$ $\mu\Omega$ cm, and a large residual resistance ratio (RRR) value $= \rho(300\text{ K})/\rho(2\text{ K}) = 104$ recorded for this sample. In the past, the low natural abundance (∼4.7%) of ^{29}Si ($I = 1/2$, $\gamma_n/2\pi = 845.77$ Hz/Oe, where γ_n is the gyromagnetic ratio) had precluded highly accurate ^{29}Si NMR measurements in $YbRh_2Si_2$. For this and previous NMR studies of this system, a single crystal sample has been prepared with the ^{29}Si isotope enriched to 52%, improving the NMR sensitivity by a factor ∼11. The standard spin-echo saturation recovery method was used for the determination of spin-lattice relaxation times T_1.

To present our two-state results for the case of field H along an a axis, we begin by briefly reviewing the basic phenomenology of this effect and the experimental analysis of T_1 data that led to its identification in the c-axis case [16]. Thus, in a FL state, Korringa relaxation $1/T_1T \sim$ const is expected, while, in contrast, in a NFL state, $1/T_1T \sim T^{-\nu}$, i.e., Im $\chi_a(q,\omega_n) \to \infty$ as $T \to 0$ K, where the value of ν depends on the type of criticality [17]. In the previous $H\|c$ case [16], the NFL behavior exhibited $\nu \sim 1$, giving regions with $T_1 \sim$ const near the QCPT. Since $T_1 \propto 1/T$ for the FL state, a substantial contrast developed between T_1 for the FL and NFL states at sufficiently low temperatures. Here, a similar effect is observed, but is confined to a lower temperature region owing to the lower QCPT energy scale with H in the basal plane.

For ^{29}Si ($I = 1/2$) the time dependence of the spin-lattice relaxation curve for nuclear magnetization $M(t)$ in a homogeneous electronic state is a simple exponential with a unique T_1,

$$\frac{M(t)}{M(\infty)} = 1 - \exp(-t/T_1). \tag{1}$$

However, in a system with two coexisting electronic states, an S state with short T_{1S} and an L state with long T_{1L}, the relaxation curve is expressed by a two-component equation,

$$\begin{aligned} \frac{M(t)}{M(\infty)} &= \frac{M_L(\infty)}{M(\infty)}\{R[1 - \exp(-t/T_{1S})] \\ &\quad + 1 - \exp(-t/T_{1L})\}, \\ M(\infty) &= M_S(\infty) + M_L(\infty), \\ R &= M_S(\infty)/M_L(\infty), \end{aligned} \tag{2}$$

*Present address: Division of Physics, Tokyo Metropolitan University, Hachioji-shi, Tokyo 192-0397, Japan.

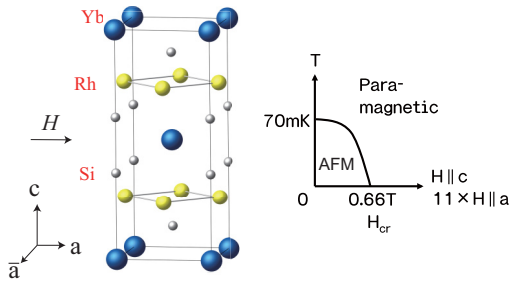

FIG. 1. (Color online) Left: Crystal structure ($I4/mmm$) of $YbRh_2Si_2$. The local symmetry of the Si site is tetragonal ($4mm$). The a and $\bar{a}$ axes are identical crystallographically; however, they are distinguishable under magnetic field $H\|a$ [13]. Right: The T-H phase diagram (PD) of $YbRh_2Si_2$. Antiferromagnetic order (AFM) disappears at H_{cr}. The PD for $H\|a$ coincides with the PD for $H\|c$ if $H\|a$ is multiplied by 11 [1].

where $M_S(\infty)$ and $M_L(\infty)$ are the S- and L-state equilibrium nuclear magnetizations, respectively. Cases where $M_S(\infty) = 0$ or $M_L(\infty) = 0$ correspond to Eq. (1). As we note below, the S and L states correspond to the NFL and FL states, respectively. The ratio R gives the proportion of S-state (NFL) to L-state (FL) nuclear magnetization in the sample. Since $M_{S,L}(\infty)$ is proportional to the respective numbers of Si in each state, R corresponds to the ratio of the NFL state fractional population $f_{\rm NFL}(T)$ to that of the FL state $f_{\rm FL}(T) = 1 - f_{\rm NFL}(T)$, i.e., $R = f_{\rm NFL}(T)/f_{\rm FL}(T)$. In the present measurements, all relaxation data obtained are fitted quite well by either Eq. (1) or (2).

Figure 2(a) shows semilogarithmic plots of $1 - M(t)/M(\infty)$ at $T = 45$ mK for different magnetic fields. A clear straight line at 7.2 T indicates a homogenous electronic state at high magnetic fields. As the field decreases, the plot curvature again indicates that two different states appear at lower fields. Figure 2(b) shows semilogarithmic plots of $1 - M(t)/M(\infty)$ at $H = 0.31$ T for different temperatures. At higher temperatures, e.g., 492 mK, a clear straight line is obtained, indicating a homogeneous state with a unique T_1. In contrast, as T decreases, the $1 - M(t)/M(\infty)$ curve is bent in a fashion that is well fitted by the two-component Eq. (2), indicating that two different states coexist at lower temperatures. This behavior is similar to that found earlier for $H\|c$ [16].

Figure 3(a) shows the T dependence of $1/T_{1L}T$ and $1/T_{1S}T$ at several magnetic fields. The present results for $H\|a$ are consistent with previous findings [18], although the two states are well separated in the present study owing to the NMR signal enhancement from the enriched sample. There are significant differences between the present $H\|a$ and previous $H\|c$ cases. In contrast to the $H\|c$ case, the unique $1/T_1(\equiv 1/T_{1L})$ depends strongly on H, beginning at temperatures as high as ~50 K. This H dependence is very likely related to the strong H dependence of static susceptibility χ_a for $H\|a$, which reflects the density of states at E_F: $\chi_a \propto D_{E_F}$. Actually, $T_{1L}(7.2\ {\rm T})/T_{1L}(0.66\ {\rm T}) \propto [D_{E_F}(0.66\ {\rm T})/D_{E_F}(7.2\ {\rm T})]^2 \sim 4$ at 2 K [Fig. 3(a)] is consistent with $[\chi_a(0.66\ {\rm T})/\chi_a(7\ {\rm T})]^2 \sim 4$ at 2 K [Fig. 3(b)], indicating that the ferromagnetic correlation [18] does not

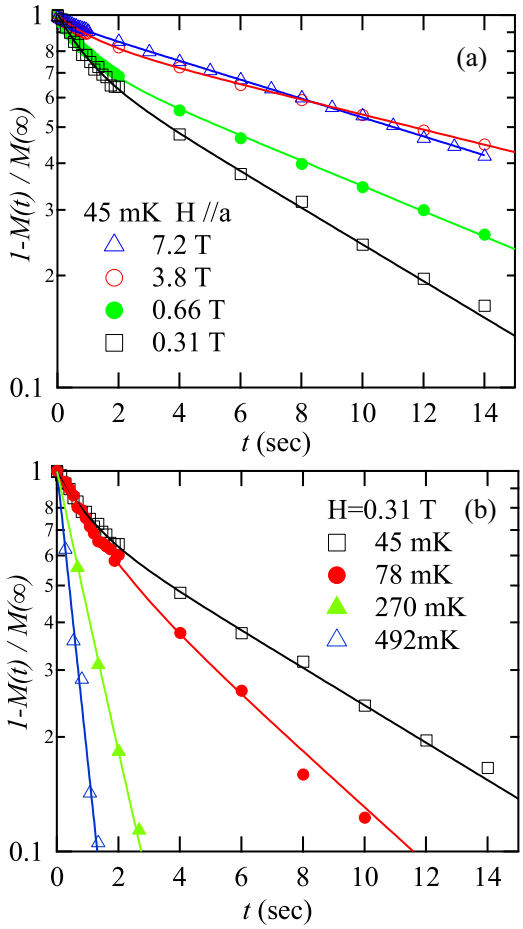

FIG. 2. (Color online) (a) Nuclear relaxation curves at $T = 45$ mK in different applied fields. Solid lines are obtained by least squares fits to Eq. (1) for 7.2 T and to Eq. (2) for 3.8, 0.66, and 0.31 T. At 7.2 T the relaxation curve is straight, indicating a homogeneous (FL) state. With decreasing field, nonlinear relaxation curves appear which are well fitted by Eq. (2), indicating the presence of two different states. (b) Nuclear magnetic relaxation curves at $H = 0.31$ T at different temperatures. Solid lines are obtained by least squares fits to Eq. (1) for 492 mK and to Eq. (2) for other temperatures. At 492 mK, the relaxation curve is a straight line, indicating a homogeneous (NFL) state. As temperature decreases, two-component relaxation curves appear, which are well fitted by Eq. (2), indicating the appearance of two different states.

depend strongly on H above 2 K. It should be noted that the static susceptibility χ_c is independent of $H\|c$ up to 7 T [16].

Since $1/T_{1L}T$ is roughly independent of T at low temperatures, the L state corresponds to the FL state. The T dependence of $1/T_{1L}T$ at 7.2 T and at low T may be the result of the fine structure at the Fermi level [19,20]. On the other hand, for the S state, $1/T_{1S}T \propto T^{-\nu}$ ($\nu \sim 1$), which corresponds to the NFL state. The present results indicate that there is a coexistence of regions exhibiting FL and localized NFL states in the sample near the QCPT, as was found with $H\|c$ [16]. Compared with the case of $H\|c$, here the NFL state, i.e., T_{1S}, appears only at very low temperatures $T < 0.1$ K and fields $H < 0.66$ T. In addition, values of $1/T_{1L}T$ increase here with decreasing H in the FL state, whereas $1/T_{1S}T$, i.e., the NFL state, seems to be independent of H.

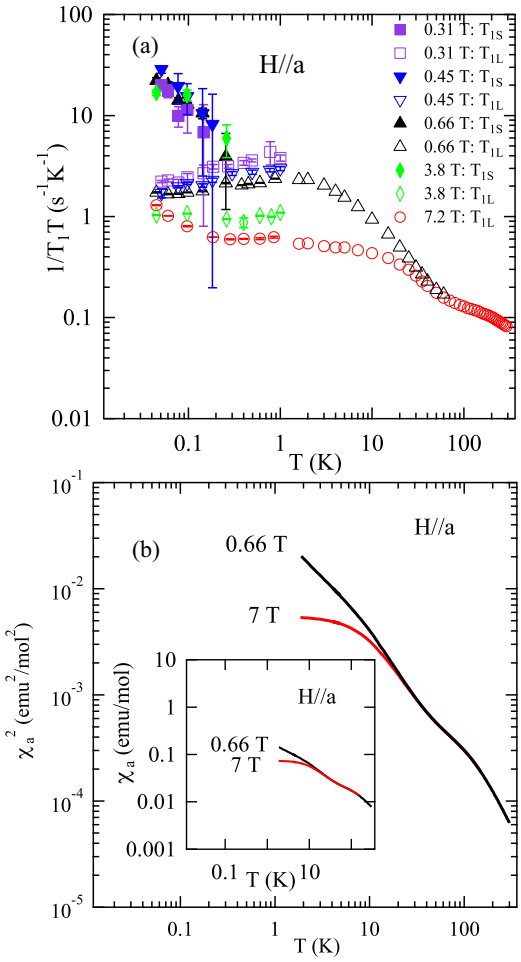

FIG. 3. (Color online) (a) T dependence of $1/T_{1S}T$ (NFL state) and $1/T_{1L}T$ (FL state) at different fields (listed in the figure). Down to ∼0.1 K no clearly resolved separate decay curves have appeared, whereas the unique $T_1(\equiv T_{1L})$ depends on H. As T decreases below ∼0.1 K at low fields, distinct values are resolved for $1/T_{1S}T$ and $1/T_{1L}T$. The experimental error for $1/T_{1S}T$ is large for T above ∼0.1 K. At the highest field, 7.2 T, only $1/T_{1L}T$ appears. (b) T dependence of squared static susceptibility χ_a^2 at 0.66 and 7 T for $H\|a$ with the same scale of T as in (a), suggesting a simple density-of-states mechanism for the field dependence of T_{1L}. The inset shows T dependence of the static susceptibility χ_a for the same data.

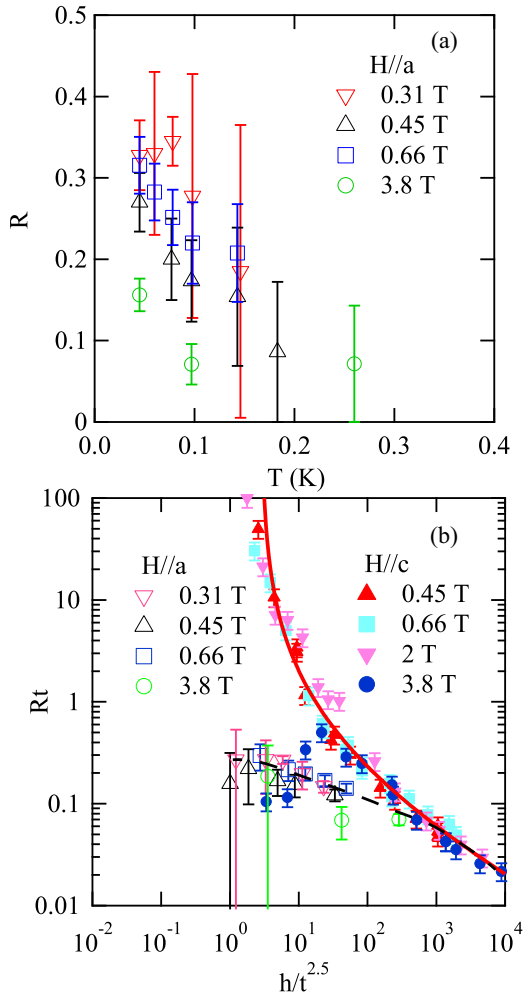

FIG. 4. (Color online) (a) T dependence of R at different fields. As shown, the experimental error at high temperatures is large, thus clearly resolved finite R is only considered to appear below ∼0.1 K. (b) Scaling plot for $H\|a$ and $H\|c$ cases. R obeys the scaling relation $Rt \sim \Phi_i(h/t^{2.5})$. The solid line represents the scaling function Φ_c obtained for the $H\|c$ case [16]. The dashed line represents the scaling function Φ_a for the present $H\|a$ case, which merges into Φ_c for $h/t^{2.5} > 10^2$. Here we adopt the estimates $T_c^\dagger/T_a^\dagger = H_c^\dagger/H_a^\dagger = 10$. As temperature and field units, $T_c^\dagger = 1$ K and $H_c^\dagger = 1$ T are employed tentatively.

In general, $1/T_1T$ is related to the dynamical susceptibilities Im $\chi(q,\omega_n)$ [21],

$$1/(T_1T) = 2\gamma_n^2 \sum_q A^2(q)\mathrm{Im}\,\chi(q,\omega_n)/\omega_n. \qquad (3)$$

Here, $A(q)$ is the transferred hyperfine coupling tensor at the Si site, and $\omega_n/2\pi = \gamma_n H/2\pi$ is the NMR measurement frequency (∼MHz). The spin-lattice relaxation of the ^{29}Si is mainly driven by magnetic fluctuations at the Yb sites conveyed by transferred hyperfine couplings. Therefore, $1/T_1T$ is a direct measure of Im $\chi(q,\omega_n)$, i.e., of the magnetic excitations at the Yb site.

In our earlier report [16], it was stated that FL excitations may originate near the ferromagnetic wave vector $q \sim 0$; in contrast, the NFL excitations may arise with an antiferromagnetic wave vector $q > 0$ in the vicinity of the antiferromagnetic ordering. Along with the static susceptibility χ_a at $q = 0$, which decreases with increasing $H\|a$ [Fig. 3(b)], the ferromagnetic Im $\chi(q \sim 0,\omega_n)$ that drives $1/T_{1L}T$ is also presumed to decrease with increasing $H\|a$. Consequently, the FL excitations $(1/T_{1L}T)$ around $q \sim 0$ show a similar field dependence. Actually, a similar field dependence of ferromagnetic excitations is observed in neutron scattering measurements [11]. On the other hand, the present field-independent NFL excitations $(1/T_{1S}T)$ indicate that antiferromagnetic Im $\chi(q > 0,\omega_n)$ is independent of $H\|a$ (as well as for $H\|c$ [16]).

Figure 4(a) displays the measured H,T dependence of R [see Eq. (2)]. Considering experimental error, a clear NFL branch appears only at $T < 0.1$ K and $H < 0.66$ T. Although $1/T_{1S}T$ from the NFL region is insensitive to the applied field

as mentioned above, the NFL fraction is suppressed rapidly by $H\|a$. From the scaling relation discussed below, a thoroughly mixed, nearly degenerate, i.e., $R \sim 1$, state for $H\|a$ is expected to appear below 20 mK and 0.2 T. Experimental results at such a low temperature are unfortunately rather limited, since the lowest possible temperature in a typical dilution refrigerator is ∼10 mK without excitation sources for measurements.

In the previous study [16], the scaling relation $RT = \Phi(H/T^{2.5})$ was found to hold for the case of $H\|c$ at low temperatures. The same scaling relation may be adopted for the present case of $H\|a$ if normalized variables temperature t and field h are used, i.e.,

$$Rt \sim \Phi_i(h/t^{2.5}), \quad t \equiv T/T_i^{\dagger}, \quad h \equiv H/H_i^{\dagger}, \qquad (4)$$

where Φ_i, $T_i^{\dagger}$, and $H_i^{\dagger}$ (i: a,c axes) are the scaling function, characteristic temperature, and field for the cases of $H\|a$,c, respectively. As shown in Fig. 4(b), the present Φ_a seems to merge into the previous Φ_c at low temperatures, i.e., above $h/t^{2.5} \sim 10^2$, if $T_c^{\dagger} \sim 10T_a^{\dagger}$ and $H_c^{\dagger} \sim 10H_a^{\dagger}$ are assumed. Below $h/t^{2.5} \sim 10^2$, Φ_a and Φ_c diverge, probably due to crossover effects. Unfortunately, measurements above $h/t^{2.5} \sim 10^2$ are difficult for the case of $H\|a$, since temperatures below 20 mK are necessary. As pointed out previously [1,4], the phase diagram of $YbRh_2Si_2$ for $H\|a$ coincides with that for $H\|c$ if the magnetic field scale is multiplied by ∼11 (Fig. 1). The present scaling behavior is consistent with this fact.

Although the origins of degenerate coexisting states and of the scaling law are still unclear, the present study confirms that the proportion of NFL to FL states R shows similar contrasting energy scales with field orientation as the previously measured physical properties around the QCPT [1,12]. This observation strongly suggests that the quantity R relates directly to quantum criticality in $YbRh_2Si_2$. As previously described [16], the two-fluid model [22] can reproduce the T dependence of R phenomenologically [solid line in Fig. 4(b)]. The locally critical model [8], the strong coupling critical model [23], and the quantum tricritical model [24] imply the coexistence of two different excitations. However, they do not envision the occurrence of separate regions of the sample that embody those two types of excitation, as we report here and in our previous paper [16]. Thus, no explicit prescription for R has been proposed. In any case, a more detailed microscopic theory for the coexisting states is greatly desired.

A confirmation of the coexisting states in transport and macroscopic measurements may be difficult to achieve, since contributions from the FL and NFL states are averaged. In contrast, microscopic electron spin resonance (ESR) [25] and Mössbauer [26] measurements probe localized and itinerant states. It may be useful to analyze microscopic muon spin rotation (μSR) relaxation curves in a single crystal sample based on the coexistence picture; up to now, only measurements in a powder sample have been reported [27].

Recently, it was reported that the appearance of heterogeneous electronic states can be controlled by pressure around a QCPT in Cd-doped (i.e., disordered) $CeCoIn_5$ [28]. Even in very pure samples of URu_2Si_2, a heterogeneous "hidden order" state appears as a result of low level disorder [29]. The relation between electronic heterogeneity and low level disorder in pure $YbRh_2Si_2$ could also be profitably addressed.

Finally, the valence states of Yb might also be different: $Yb^{(3-\delta)+}$ for the FL state and Yb^{3+} for the NFL state, so that the QCPT of $YbRh_2Si_2$ may be near a valence instability [30]. In this context, it would be crucial to identify the order parameter of the ordered state in order to elucidate the exotic QCPT.

We are grateful for stimulating discussions with S. Watanabe, K. Izawa, K. Ishida, N. Tateiwa, and H. Ikeda. A part of this work was supported by a Grant-in-Aid for Scientific Research on Innovative Areas "Heavy Electrons" (No. 20102006 and No. 20102007) by the Ministry of education, culture, sports, science & technology in Japan, and the REIMEI Research Program of JAEA.

[1] P. Gegenwart, J. Custers, C. Geibel, K. Neumaier, T. Tayama, K. Tenya, O. Trovarelli, and F. Steglich, Phys. Rev. Lett. **89**, 056402 (2002).

[2] S. Paschen, T. Lühmann, S. Wirth, P. Gegenwart, O. Trovarelli, C. Geibel, F. Steglich, P. Coleman, and Q. Si, Nature (London) **432**, 881 (2004).

[3] S. Friedemann, T. Westerkamp, M. Brando, N. Oeschler, S. Wirth, P. Gegenwart, C. Krellner, C. Geibel, and F. Steglich, Proc. Natl. Acad. Sci. USA **107**, 14547 (2010).

[4] P. Gegenwart, Q. Si, and F. Steglich, Nat. Phys. **4**, 186 (2008).

[5] O. Trovarelli, C. Geibel, S. Mederle, C. Langhammer, F. M. Grosche, P. Gegenwart, M. Lang, G. Sparn, and F. Steglich, Phys. Rev. Lett. **85**, 626 (2000).

[6] S. Ernst, S. Kirchner, C. Krellner, C. Geibel, G. Zwicknagl, F. Steglich, and S. Wirth, Nature (London) **474**, 362 (2011).

[7] A. J. Millis, Phys. Rev. B **48**, 7183 (1993).

[8] Q. Si, S. Rabello, K. Ingersent, and J. L. Smith, Nature (London) **413**, 804 (2001).

[9] P. Coleman, C. Pépin, Q. Si, and R. Ramazashvili, J. Phys.: Condens. Matter **13**, R723 (2001).

[10] C. Pépin, Phys. Rev. Lett. **98**, 206401 (2007).

[11] C. Stock, C. Broholm, F. Demmel, J. Van Duijn, J. W. Taylor, H. J. Kang, R. Hu, and C. Petrovic, Phys. Rev. Lett. **109**, 127201 (2012).

[12] J. Custers, P. Gegenwart, H. Wilhelm, K. Neumaier, Y. Tokiwa, O. Trovarelli, C. Geibel, F. Steglich, C. Pépin, and P. Coleman, Nature (London) **424**, 524 (2003).

[13] S. Kambe, H. Sakai, Y. Tokunaga, G. Lapertot, T. D. Matsuda, G. Knebel, J. Flouquet, and R. E. Walstedt, J. Phys.: Conf. Ser. **592**, 012085 (2015).

[14] H. Pfau, S. Hartmann, U. Stockert, P. Sun, S. Lausberg, M. Brando, S. Friedemann, C. Krellner, C. Geibel, S. Wirth, S. Kirchner, E. Abrahams, Q. Si, and F. Steglich, Nature (London) **484**, 493 (2012).

[15] K. Kummer, S. Patil, A. Chikina, M. Güttler, M. Höppner, A. Generalov, S. Danzenbächer, S. Seiro, A. Hannaske, C. Krellner, Yu. Kucherenko, M. Shi, M. Radovic, E. Rienks, G. Zwicknagl,

K. Matho, J. W. Allen, C. Laubschat, C. Geibel, and D. V. Vyalikh, Phys. Rev. X **5**, 011028 (2015).

[16] S. Kambe, H. Sakai, Y. Tokunaga, G. Lapertot, T. D. Matsuda, G. Knebel, J. Flouquet, and R. E. Walstedt, Nat. Phys. **10**, 840 (2014).

[17] A. Ishigaki and T. Moriya, J. Phys. Soc. Jpn. **67**, 3924 (1998).

[18] K. Ishida, K. Okamoto, Y. Kawasaki, Y. Kitaoka, O. Trovarelli, C. Geibel, and F. Steglich, Phys. Rev. Lett. **89**, 107202 (2002).

[19] P. M. C. Rourke, A. McCollam, G. Lapertot, G. Knebel, J. Flouquet, and S. R. Julian, Phys. Rev. Lett. **101**, 237205 (2008).

[20] A. Pourret, G. Knebel, T. D. Matsuda, G. Lapertot, and J. Flouquet, J. Phys. Soc. Jpn. **82**, 053704 (2013).

[21] T. Moriya, Prog. Theor. Phys. **16**, 23 (1956).

[22] Y.-F. Yang and D. Pines, Phys. Rev. Lett. **100**, 096404 (2008).

[23] E. Abrahams, J. Schmalian, and P. Wölfle, Phys. Rev. B **90**, 045105 (2014).

[24] T. Misawa, Y. Yamaji, and M. Imada, J. Phys. Soc. Jpn. **77**, 093712 (2008).

[25] J. Sichelschmidt, V. A. Ivanshin, J. Ferstl, C. Geibel, and F. Steglich, Phys. Rev. Lett. **91**, 156401 (2003).

[26] G. Knebel, R. Boursier, E. Hassinger, G. Lapertot, P. G. Niklowitz, A. Pourret, B. Salce, J. P. Sanchez, I. Sheikin, P. Bonville, H. Harima, and J. Flouquet, J. Phys. Soc. Jpn. **75**, 114709 (2006).

[27] K. Ishida, D. E. MacLaughlin, Ben-Li Young, K. Okamoto, Y. Kawasaki, Y. Kitaoka, G. J. Nieuwenhuys, R. H. Heffner, O. O. Bernal, W. Higemoto, A. Koda, R. Kadono, O. Trovarelli, C. Geibel, and F. Steglich, Phys. Rev. B **68**, 184401 (2003).

[28] S. Seo, X. Lu, J.-X. Zhu, R. R. Urbano, N. Curro, E. D. Bauer, V. A. Sidorov, L. D. Pham, T. Park, Z. Fisk, and J. D. Thompson, Nat. Phys. **10**, 120 (2014).

[29] S. Kambe, Y. Tokunaga, H. Sakai, and R. E. Walstedt, Phys. Rev. B **91**, 035111 (2015).

[30] S. Watanabe and K. Miyake, Phys. Rev. Lett. **105**, 186403 (2010).